Geometric multigrid methods for Darcy–Forchheimer flow in fractured porous media

A. Arrarás[a], F.J. Gaspar[b,c], L. Portero[a,*], C. Rodrigo[b]

[a] *Departamento de Estadística, Informática y Matemáticas, Universidad Pública de Navarra, Edificio de Las Encinas, Campus de Arrosadía, 31006 Pamplona, Spain*
[b] *IUMA, Departamento de Matemática Aplicada, Universidad de Zaragoza, Pedro Cerbuna 12, 50009 Zaragoza, Spain*
[c] *Centrum Wiskunde & Informatica (CWI), 1098 XG Amsterdam, The Netherlands*

Abstract

In this paper, we present a monolithic multigrid method for the efficient solution of flow problems in fractured porous media. Specifically, we consider a mixed-dimensional model which couples Darcy flow in the porous matrix with Forchheimer flow within the fractures. A suitable finite volume discretization permits to reduce the coupled problem to a system of nonlinear equations with a saddle point structure. In order to solve this system, we propose a full approximation scheme (FAS) multigrid solver that appropriately deals with the mixed-dimensional nature of the problem by using mixed-dimensional smoothing and inter-grid transfer operators. Numerical experiments show that the proposed multigrid method is robust with respect to the fracture permeability, the Forchheimer coefficient and the mesh size. The case of several possibly intersecting fractures in a heterogeneous porous medium is also discussed.

Keywords: Darcy–Forchheimer, finite volumes, fractured porous media, geometric multigrid
2010 MSC: 65F10, 65N22, 65N55, 76S05

1. Introduction

Modeling and simulation of fluid flow in fractured porous media is a challenging task which is getting increasing attention in recent years, due to the wide range of applications in which plays an essential role. Different fracture models have been proposed in the last decades based on the spatial scale under consideration and the knowledge of the fracture distribution. On the one hand, double-continuum models are suitable for regularly distributed micro-fractures showing interconnections with the surrounding matrix. Such models assume

*Corresponding author.
Email addresses: andres.arraras@unavarra.es (A. Arrarás), fjgaspar@unizar.es (F.J. Gaspar), laura.portero@unavarra.es (L. Portero), carmenr@unizar.es (C. Rodrigo)

the existence of a mass transfer function between the bulk and the fractures [1], and are usually derived via homogenization theory [2]. On the other hand, discrete fracture networks consider sets of individual macro-fractures which are isolated from the porous matrix [3, 4]. Typically, these networks are obtained stochastically and provide information about the orientation, density, size and hydrological properties of the fractures [5]. In these latter models, fluid exchange between the fractures and the matrix is not allowed, so that flow is restricted to the fracture network. If we properly combine the preceding models, we may construct what we refer to as discrete fracture-matrix models: sets of individual macro-fractures, similar to those arising in discrete fracture networks, but suitably coupled with the surrounding matrix, as in double-continuum models. These are the models considered in this paper. More precisely, we suppose that fractures can be represented as $(n-1)$-dimensional interfaces immersed into an n-dimensional porous matrix, thus giving rise to the so-called mixed-dimensional or interface models [6, 7].

Most earlier works using this approach suppose that the flow within the fractures and in the porous matrix is described by Darcy's law [8, 9, 10]. Darcy's law has been shown to govern single-phase incompressible flow in porous media at specific flow regimes where the velocity is low. This is the case, for example, of subsurface reservoirs and aquifers, where a low permeability of the porous matrix implies low velocities. However, in proximity to wellbores or within high-permeability fractures, velocities are higher, thus requiring the use of alternative nonlinear flow models [11]. The simplest of such models is based on the addition of a quadratic correction term in the velocity to the linear Darcy model. The new model, referred to as Forchheimer's law, combines the contribution of viscous and inertial effects: at low flow rates, the viscous effect is dominant and the model reduces to Darcy's law; at increasing flow rates, however, the inertial effect gains relevance and plays a significant role [12]. Remarkably, other nonlinear correction terms –e.g., cubic [13], polynomial [11] or exponential [14]– have also been proposed in the literature.

The validity of Forchheimer's law in a certain range of velocities for laminar flow has been established empirically (see [15, 16] and references therein). From a theoretical viewpoint, the Forchheimer model has been deduced using homogenization methods [17, 18], volume averaging [19, 20], and related techniques [21]. Existence, uniqueness and regularity results have been derived in [22, 23, 24]. Numerically, different strategies –ranging from mixed finite elements [25, 26, 27] to block-centered finite differences [28, 29] and multipoint flux approximation methods [30]– have been applied to obtain approximate solutions of this model.

In this work, we are concerned with the numerical solution of a discrete fracture-matrix model which couples Darcy flow in the porous matrix with Forchheimer flow within the fractures. The solvability of this problem is analyzed in [31]. In [32, 33], numerical approximations are obtained using the lowest order Raviart–Thomas mixed finite elements in combination with a domain decomposition technique. In both works, the nonlinear system stemming from the Forchheimer equation is solved using fixed-point iteration and quasi-Newton methods. Alternative efficient solvers for various discretizations

of the isolated Forchheimer model include the Peaceman–Rachford iteration scheme [34], different variants of the two-grid method [35, 36], and a multigrid method based on the so-called full approximation scheme (FAS) [37]. In the spirit of this latter work, we propose a monolithic mixed-dimensional multigrid method that extends our earlier work [38] for the Darcy–Darcy coupling to the Darcy–Forchheimer case. Note that, in this case, the mixed-dimensional approach establishes a connection between dimensionality and nonlinearity: an n-dimensional linear Darcy problem is coupled with an $(n-1)$-dimensional nonlinear Forchheimer problem. For the discretization, we consider a finite volume method that combines control volumes of different dimensions in the fractures and the porous matrix. The nonlinear system stemming from the discretization has a saddle point structure, and can be suitably handled using the FAS multigrid solver [39].

Multigrid methods are well known to be among the fastest solvers for the solution of linear and nonlinear systems of equations, showing very often optimal computational cost and convergence behavior [40]. The performance of multigrid algorithms strongly depends on the choice of their components, so that many details are open for discussion and decision in the design of a multigrid method for a target problem. In the framework considered here, where a mixed-dimensional problem needs to be solved, it seems natural to combine two-dimensional smoothing and inter-grid transfer operators for the unknowns in the porous matrix with their one-dimensional counterparts within the fracture network. Regarding the smoother, due to the saddle point character of the resulting system, a Vanka-type relaxation is proposed for both the unknowns in the porous matrix and within the fractures. This class of smoothers was firstly proposed by Vanka in [41] for the multigrid solution of the staggered finite difference discretization of the Navier–Stokes equations and, since then, it has been applied to different problems in both computational fluid and solid mechanics. In particular, here we consider a standard two-dimensional five-point Vanka smoother for the unknowns in the porous matrix, and a variant of its one-dimensional three-point nonlinear counterpart for those unknowns within the fractures. The proposed relaxation procedure simultaneously updates the fracture unknowns at one cell within the fracture with those two velocities from the porous matrix located at the edges of the corresponding two-dimensional elements that match at that particular fracture cell. The inter-grid transfer operators that act on the different unknowns are dictated by the corresponding one- and two-dimensional staggered location of the grid points within the fractures and the porous matrix, respectively. The proposed mixed-dimensional multigrid method is shown to be robust with respect to the fracture permeability, the mesh size, and the so-called Forchheimer coefficient, which represents a measure of the strength of the nonlinearity (see problem (1)). In addition, robustness is preserved for a fracture network with several possibly intersecting fractures, in heterogeneous porous media, and at different injection rates within the fractures.

The rest of the paper is organized as follows. In Section 2, we describe the discrete fracture-matrix model coupling Darcy flow in the porous matrix

with Forchheimer flow in the fractures. The finite volume spatial discretization is formulated in Section 3, where we further specify the resulting nonlinear system of algebraic equations. In Section 4, we introduce a monolithic mixed-dimensional multigrid method for solving such a system. Finally, we report a collection of numerical experiments in Section 5, illustrating the robustness of the proposed method with respect to different parameters.

2. The continuous problem

Let $\Omega \subset \mathbb{R}^2$ be an open, bounded, and convex polygonal domain, whose boundary is denoted by $\Gamma = \partial\Omega$. We consider a single-phase incompressible flow in Ω governed by the mass conservation equation, together with Forchheimer's law that relates the gradient of the pressure p to the flow velocity $\mathbf{u}$, i.e.,

$$\begin{aligned} (1 + \beta\,|\mathbf{u}|)\,\mathbf{u} &= -\mathbf{K}\nabla p && \text{in } \Omega, \\ \nabla \cdot \mathbf{u} &= q && \text{in } \Omega, \\ p &= 0 && \text{on } \Gamma. \end{aligned} \tag{1}$$

Here, β represents the dynamic viscosity or Forchheimer coefficient, and is supposed to be a scalar, $\mathbf{K} \in \mathbb{R}^{2\times 2}$ is the permeability tensor, and q is a source/sink term. We suppose that $\mathbf{K}$ is a diagonal tensor whose entries K_{xx} and K_{yy} are strictly positive and bounded in Ω. For the sake of convenience, homogeneous Dirichlet boundary conditions are considered, but other types of boundary data can also be handled. We further assume that the porous medium Ω contains a subset Ω_f representing a single fracture, which divides the flow domain into two disjoint connected subdomains Ω_1 and Ω_2, i.e.,

$$\Omega \backslash \overline{\Omega}_f = \Omega_1 \cup \Omega_2, \qquad \Omega_1 \cap \Omega_2 = \emptyset.$$

In addition, we introduce the notations $\Gamma_k = \partial\Omega_k \cap \Gamma$, for $k = 1, 2, f$, and $\gamma_k = \partial\Omega_k \cap \partial\Omega_f \cap \Omega$, for $k = 1, 2$. The unit vector normal to γ_k pointing outward from Ω_k is denoted by $\mathbf{n}_k$, for $k = 1, 2$. A schematic representation of the flow domain including the previous notations is shown in Figure 1 (left).

Following [33], we assume that the velocity in the subdomains is small enough to be described by Darcy's law, while that in the fracture needs to be modeled by Forchheimer's law. Under these assumptions, problem (1) may be rewritten as the following transmission problem, for $k = 1, 2, f$, and $j = 1, 2$

$$\mathbf{u}_j = -\mathbf{K}_j \nabla p_j \qquad \text{in } \Omega_j, \tag{2a}$$
$$(1 + \beta\,|\mathbf{u}_f|)\,\mathbf{u}_f = -\mathbf{K}_f \nabla p_f \qquad \text{in } \Omega_f, \tag{2b}$$
$$\nabla \cdot \mathbf{u}_k = q_k \qquad \text{in } \Omega_k, \tag{2c}$$
$$p_j = p_f \qquad \text{on } \gamma_j, \tag{2d}$$
$$\mathbf{u}_j \cdot \mathbf{n}_j = \mathbf{u}_f \cdot \mathbf{n}_j \qquad \text{on } \gamma_j, \tag{2e}$$
$$p_k = 0 \qquad \text{on } \Gamma_k, \tag{2f}$$

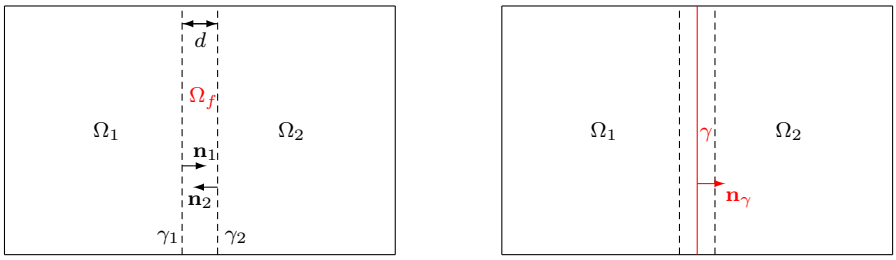

Figure 1: Schematic representation of the original domain (left) and the reduced domain (right).

where p_k, $\mathbf{u}_k$, $\mathbf{K}_k$ and q_k are the restrictions of p, $\mathbf{u}$, $\mathbf{K}$ and q, respectively, to Ω_k, for $k = 1, 2, f$. The equations (2d) and (2e) provide coupling conditions that guarantee the continuity of the pressure and the normal flux, respectively, across the interfaces between the fracture and the porous matrix.

In the preceding transmission problem, both the bulk and the fracture are defined to be two-dimensional domains. As a consequence, from a numerical viewpoint, we will need extremely fine meshing to resolve the width of the fracture, assumed to be much smaller than its length. This fact will thus increase the computational cost of the algorithm. In order to circumvent this drawback, the fracture is considered to be a one-dimensional interface between the bulk subdomains Ω_1 and Ω_2. The resulting model is known as mixed-dimensional or reduced model. This idea was first proposed in [7] for a Darcy–Darcy coupling between the fracture and the porous matrix, and has been subsequently used in [31, 32, 33] in the context of Darcy–Forchheimer couplings. Note that, as an additional advantage in this latter case, the nonlinear Forchheimer problem (2b) posed in the fracture is no longer a two-dimensional problem, but a one-dimensional one.

According to [7], there exists a non-self-intersecting one-dimensional manifold γ such that the fracture can be expressed as

$$\Omega_f = \left\{ \mathbf{x} \in \Omega : \mathbf{x} = \mathbf{s} + \theta\, \mathbf{n}_\gamma, \text{ for some } \mathbf{s} \in \gamma \text{ and } |\theta| < \frac{d(\mathbf{s})}{2} \right\},$$

where $d(\mathbf{s}) > 0$ denotes the width of the fracture at $\mathbf{s}$ in the normal direction, and $\mathbf{n}_\gamma$ is the outward unit normal to γ with a fixed orientation from Ω_1 to Ω_2. Note that, with this definition, $\mathbf{n}_\gamma = \mathbf{n}_1 = -\mathbf{n}_2$ (see Figure 1). We will suppose that $d(\mathbf{s})$ is much smaller than the other characteristic dimensions of the fracture.

The key point in this procedure is to collapse the fracture Ω_f into the line γ, and integrate the equations (2b) and (2c) (the latter for the index $k = f$) along the fracture width. In doing so, we need to split up such equations into their normal and tangential parts. Let us denote the projection operators onto the normal and tangent spaces of γ as $\mathbf{P_n} = \mathbf{n}_\gamma \mathbf{n}_\gamma^T$ and $\mathbf{P}_{\boldsymbol{\tau}} = \mathbf{I} - \mathbf{P_n}$, $\mathbf{I}$ being

the identity tensor. For regular vector- and scalar-valued functions $\mathbf{g}$ and g, the tangential divergence and gradient operators on the fracture are defined, respectively, as

$$\nabla^{\boldsymbol{\tau}} \cdot \mathbf{g} = \mathbf{P}_{\boldsymbol{\tau}} : \nabla \mathbf{g}, \qquad \nabla^{\boldsymbol{\tau}} g = \mathbf{P}_{\boldsymbol{\tau}} \nabla g.$$

Following [3], we assume that the permeability tensor $\mathbf{K}_f$ decomposes additively as

$$\mathbf{K}_f = K_f^{\mathbf{n}} \mathbf{P}_{\mathbf{n}} + K_f^{\boldsymbol{\tau}} \mathbf{P}_{\boldsymbol{\tau}}, \tag{3}$$

where $K_f^{\mathbf{n}}$ and $K_f^{\boldsymbol{\tau}}$ are defined to be strictly positive and bounded in Ω_f. Accordingly, $\mathbf{u}_f = \mathbf{u}_{f,\boldsymbol{\tau}} + \mathbf{u}_{f,\mathbf{n}}$, where $\mathbf{u}_{f,\boldsymbol{\tau}} = \mathbf{P}_{\boldsymbol{\tau}} \mathbf{u}_f$ and $\mathbf{u}_{f,\mathbf{n}} = \mathbf{P}_{\mathbf{n}} \mathbf{u}_f$.

In this framework, we introduce the so-called reduced variables, namely: the reduced pressure p_γ, the reduced Darcy velocity $\mathbf{u}_\gamma$, and the reduced source/sink term q_γ, formally defined as [7, 9]

$$p_\gamma(\mathbf{s}) = \frac{1}{d(\mathbf{s})}(p_f, 1)_{\ell(\mathbf{s})}, \qquad \mathbf{u}_\gamma(\mathbf{s}) = (\mathbf{u}_{f,\boldsymbol{\tau}}, 1)_{\ell(\mathbf{s})}, \qquad q_\gamma(\mathbf{s}) = (q_f, 1)_{\ell(\mathbf{s})},$$

where $\ell(\mathbf{s}) = \left(-\frac{d(\mathbf{s})}{2}, \frac{d(\mathbf{s})}{2}\right)$. In addition, along the lines of [33], we assume that the flow in the normal direction within the fracture is described by Darcy's law. This assumption is based on the fact that the ratio between the width and the length of the fracture is small. Thus, equation (2b) may be decomposed into its tangential and normal direction as follows

$$(1 + \beta \, |\mathbf{u}_f|) \, \mathbf{u}_{f,\boldsymbol{\tau}} = -K_f^{\boldsymbol{\tau}} \, \nabla^{\boldsymbol{\tau}} p_f, \tag{4a}$$

$$\mathbf{u}_{f,\mathbf{n}} = -K_f^{\mathbf{n}} \, \nabla^{\mathbf{n}} p_f. \tag{4b}$$

Since $\mathbf{u}_{f,\mathbf{n}}$ is assumed to be much smaller than $\mathbf{u}_{f,\boldsymbol{\tau}}$, we have the approximation $|\mathbf{u}_f| \approx |\mathbf{u}_{f,\boldsymbol{\tau}}| \approx \frac{1}{d} |\mathbf{u}_\gamma|$. Then, the integration of (4a) along the line segment $\ell(\mathbf{s})$ permits us to derive a Forchheimer's law in the one-dimensional domain γ. In turn, the integration of (4b) in the normal direction to the fracture can be used to give boundary conditions along γ for the systems in Ω_1 and Ω_2. Hence, we obtain the following interface problem, for $k = 1, 2$,

$$\mathbf{u}_k = -\mathbf{K}_k \nabla p_k \qquad \text{in } \Omega_k, \tag{5a}$$

$$\nabla \cdot \mathbf{u}_k = q_k \qquad \text{in } \Omega_k, \tag{5b}$$

$$\left(1 + \frac{\beta}{d} \, |\mathbf{u}_\gamma|\right) \mathbf{u}_\gamma = -d K_f^{\boldsymbol{\tau}} \nabla^{\boldsymbol{\tau}} p_\gamma \qquad \text{on } \gamma, \tag{5c}$$

$$\nabla^{\boldsymbol{\tau}} \cdot \mathbf{u}_\gamma = q_\gamma + (\mathbf{u}_1 \cdot \mathbf{n}_1 + \mathbf{u}_2 \cdot \mathbf{n}_2) \qquad \text{on } \gamma, \tag{5d}$$

$$\alpha_\gamma (p_k - p_\gamma) = \xi \, \mathbf{u}_k \cdot \mathbf{n}_k - (1 - \xi) \, \mathbf{u}_{k+1} \cdot \mathbf{n}_{k+1} \qquad \text{on } \gamma, \tag{5e}$$

$$p_k = 0 \qquad \text{on } \Gamma_k, \tag{5f}$$

$$p_\gamma = 0 \qquad \text{on } \partial\gamma, \tag{5g}$$

where $\alpha_\gamma = 2K_f^{\mathbf{n}}/d$ and the index k is supposed to vary in $\mathbb{Z}/2\mathbb{Z}$, so that, if $k = 2$, then $k + 1 = 1$. According to [7, 42], $\xi \in (1/2, 1]$ is a closure parameter related to the pressure cross profile in the fracture. The ratio $K_f^{\mathbf{n}}/d$ and the

product $K_f^\tau d$ are sometimes referred to as effective permeabilities in the normal and tangential directions to the fracture, respectively [8].

In the preceding system, (5c) represents Forchheimer's law in the tangential direction to the fracture, while (5d) models mass conservation inside the fracture. Remarkably, the additional source term $\mathbf{u}_1 \cdot \mathbf{n}_1 + \mathbf{u}_2 \cdot \mathbf{n}_2$ is introduced on γ to take into account the contribution of the subdomain flows to the fracture flow. In turn, (5e) is obtained by averaging the equation (4b) in the normal direction to the fracture and using a quadrature rule with weights ξ and $1-\xi$ for integrating $\mathbf{u}_f \cdot \mathbf{n}_k$ across the fracture, for $k = 1, 2$. Formally, it can be regarded as a Robin boundary condition for the subdomain Ω_k that involves the pressure in the fracture p_γ and the normal flux from the neighboring subdomain Ω_{k+1}. It is quite usual to express (5e) in terms of average operators for the pressures and normal fluxes, and jump operators for the pressures across the fracture [9, 43].

3. The spatial discretization

Let us assume that the subdomains Ω_k admit rectangular partitions $\mathcal{T}_h^k$, for $k = 1, 2$, that match at the interface γ. Such meshes $\mathcal{T}_h^k$ induce a unique partition on γ denoted by $\mathcal{T}_h^\gamma$. In the case of considering a vertical fracture as that shown in Figure 1, such partitions may be defined as $\mathcal{T}_h^k = \cup_{i,j=1}^{N+1} E_{i,j}^k$ and $\mathcal{T}_h^\gamma = \cup_{j=1}^{N+1} E_j^\gamma$, where

$$E_{i,j}^k = (x_{i-1/2}^k, x_{i+1/2}^k) \times (y_{j-1/2}, y_{j+1/2}),$$
$$E_j^\gamma = \{x_\gamma\} \times (y_{j-1/2}, y_{j+1/2}),$$

x_γ being equal to $x_{N+3/2}^1$ and $x_{1/2}^2$. In the framework of finite volume methods, these sets are known as control volumes. Figure 2 shows the control volumes $E_{2,N}^1$, $E_{2,N}^2$ and E_N^γ highlighted in blue. Note that both $E_{2,N}^1$ and $E_{2,N}^2$ are two-dimensional control volumes, while E_N^γ is one-dimensional.

In this setting, we associate the pressure unknowns $p_{i,j}^k$ and p_j^γ to the element centers (x_i^k, y_j) and (x_γ, y_j), respectively, as indicated with cross signs in Figure 2. In particular,

$$p_{i,j}^k \approx \frac{1}{|E_{i,j}^k|} \iint_{E_{i,j}^k} p(x,y)\, dx\, dy, \qquad p_j^\gamma \approx \frac{1}{|E_j^\gamma|} \int_{E_j^\gamma} p_\gamma(s)\, ds.$$

In order to introduce the velocity unknowns, we first define some additional control volumes associated to the midpoints of the edges of the meshes $\mathcal{T}_h^k$, for $k = 1, 2$, and $\mathcal{T}_h^\gamma$. In particular, let us define the following control volumes associated to the vertical edges of $\mathcal{T}_h^k$,

$$E_{i+1/2,j}^k = (x_i^k, x_{i+1}^k) \times (y_{j-1/2}, y_{j+1/2}), \qquad i = 1, \ldots, N,\ j = 1, \ldots, N+1,$$
$$E_{1/2,j}^k = (x_{1/2}^k, x_1^k) \times (y_{j-1/2}, y_{j+1/2}), \qquad j = 1, \ldots, N+1,$$
$$E_{N+3/2,j}^k = (x_{N+1}^k, x_{N+3/2}^k) \times (y_{j-1/2}, y_{j+1/2}), \qquad j = 1, \ldots, N+1.$$

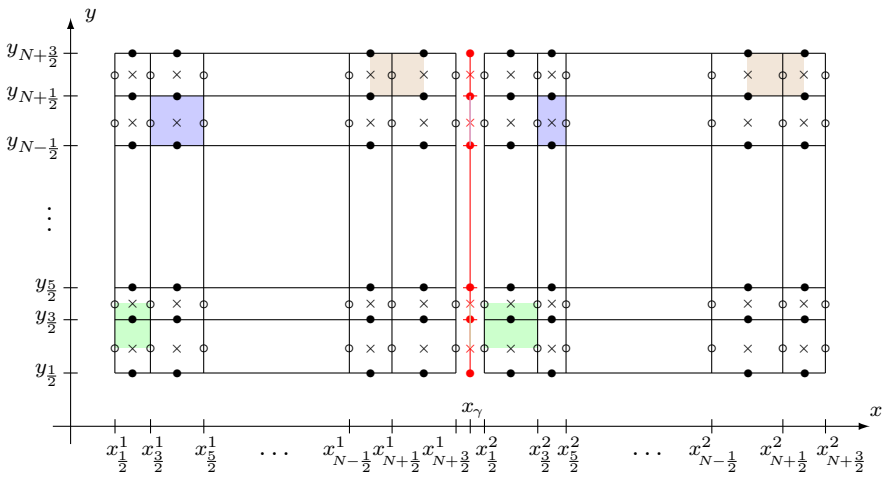

Figure 2: Staggered grid location of unknowns and corresponding control volumes.

The control volumes associated to the horizontal edges of $\mathcal{T}_h^k$ are denoted by $E^k_{i,j+1/2}$, for $i = 1, \ldots, N+1$ and $j = 0, 1, \ldots, N+1$, and may be defined in a similar way. Finally, we define the following one-dimensional control volumes associated to the mesh points $(x_\gamma, y_{j+1/2})$ of the partition $\mathcal{T}_h^\gamma$,

$$
\begin{aligned}
E^\gamma_{j+1/2} &= \{x_\gamma\} \times (y_j, y_{j+1}), \qquad j = 1, \ldots, N, \\
E^\gamma_{1/2} &= \{x_\gamma\} \times (y_{1/2}, y_1), \\
E^\gamma_{N+3/2} &= \{x_\gamma\} \times (y_{N+1}, y_{N+3/2}).
\end{aligned}
$$

Figure 2 shows the control volumes $E^1_{N+1/2,N+1}$ and $E^2_{N+1/2,N+1}$ highlighted in brown, and the control volumes $E^1_{1,3/2}$, $E^2_{1,3/2}$ and $E^\gamma_{3/2}$ highlighted in green.

In this context, the velocity unknowns can be classified into three groups. The first group comprises the normal flux components associated to the vertical edges of the two-dimensional grids $\mathcal{T}_h^k$, which are denoted by $u^k_{i+1/2,j}$, for $i = 0, 1, \ldots, N+1$, $j = 1, \ldots, N+1$, $k = 1, 2$, and are represented by black empty circles in Figure 2. The second set contains the normal flux components associated to the horizontal edges of $\mathcal{T}_h^k$, which are denoted by $v^k_{i,j+1/2}$, for $i = 1, \ldots, N+1$, $j = 0, 1, \ldots, N+1$, $k = 1, 2$, and are depicted by black filled dots in the same plot. Finally, the third group comprises the normal flux components associated to the edges of the one-dimensional grid $\mathcal{T}_h^\gamma$, which are denoted by $u^\gamma_{j+1/2}$, for $j = 0, 1, \ldots, N+1$, and are marked by red filled dots. In

particular,

$$u^k_{i+1/2,j} \approx \frac{1}{|E^k_{i+1/2,j}|} \iint_{E^k_{i+1/2,j}} u^k(x,y)\,dx\,dy,$$

$$v^k_{i,j+1/2} \approx \frac{1}{|E^k_{i,j+1/2}|} \iint_{E^k_{i,j+1/2}} v^k(x,y)\,dx\,dy,$$

$$u^\gamma_{j+1/2} \approx \frac{1}{|E^\gamma_{j+1/2}|} \int_{E^\gamma_{j+1/2}} u^\gamma(s)\,ds.$$

Let us introduce the notation $\mathbf{u}^k = (u^k, v^k)^T$ for the two components of the velocity on Ω_k, for $k = 1, 2$. Taking into account that $\mathbf{K}_k$ are diagonal tensors, with diagonal coefficients K^k_{xx} and K^k_{yy}, the equation (5a) can be decomposed as

$$u^k + K^k_{xx}\,\frac{\partial p_k}{\partial x} = 0, \tag{6a}$$

$$v^k + K^k_{yy}\,\frac{\partial p_k}{\partial y} = 0. \tag{6b}$$

The integration of equation (6a) over the control volumes $E^k_{i-1/2,j}$, together with the application of the midpoint quadrature rule in the x-direction and a suitable approximation of the flux at the midpoints of the cell edges, gives rise to the discrete equations for the horizontal velocities. In this case, we consider that the flux over each edge is approximated by using the pressure unknowns in the two cells sharing that edge. This scheme, known as the two-point flux approximation method [44], is widely used in reservoir simulations. In turn, the discrete equations for the vertical velocities are obtained by integrating equation (6b) over the control volumes $E_{i,j-1/2}$ and following a similar procedure.

In particular, the interior velocity unknowns will satisfy the following equations

$$u^k_{i-1/2,j} + 2\left(\frac{\Delta x^k_{i-1}}{(K^k_{xx})_{i-1,j}} + \frac{\Delta x^k_i}{(K^k_{xx})_{i,j}}\right)^{-1}(p^k_{i,j} - p^k_{i-1,j}) = 0,$$

$$v^k_{i,j-1/2} + 2\left(\frac{\Delta y_{j-1}}{(K^k_{yy})_{i,j-1}} + \frac{\Delta y_j}{(K^k_{yy})_{i,j}}\right)^{-1}(p^k_{i,j} - p^k_{i,j-1}) = 0,$$

where $\Delta x^k_i = x^k_{i+1/2} - x^k_{i-1/2}$ and $\Delta y_j = y_{j+1/2} - y_{j-1/2}$. Finally, integrating equation (5b) over the control volumes $E^k_{i,j}$ and applying the divergence theorem, we get

$$\frac{u^k_{i+1/2,j} - u^k_{i-1/2,j}}{\Delta x^k_i} + \frac{v^k_{i,j+1/2} - v^k_{i,j-1/2}}{\Delta y_j} = q^k_{i,j},$$

where

$$q^k_{i,j} = \frac{1}{\Delta x^k_i\,\Delta y_j} \iint_{E^k_{i,j}} q_k\,dx\,dy.$$

Similarly, by integrating equations (5c) and (5d) over the control volumes $E^{\gamma}_{j-1/2}$ and E^{γ}_{j}, respectively, we get the following equations for the interior unknowns of γ

$$\left(1+\frac{\beta}{d}|u^{\gamma}_{j-1/2}|\right)u^{\gamma}_{j-1/2}+2\,d\left(\frac{\Delta y_{j-1}}{(K^{\tau}_{f})_{j-1}}+\frac{\Delta y_{j}}{(K^{\tau}_{f})_{j}}\right)^{-1}(p^{\gamma}_{j}-p^{\gamma}_{j-1})=0,$$

$$\frac{u^{\gamma}_{j+1/2}-u^{\gamma}_{j-1/2}}{\Delta y_j}-(u^{1}_{N+3/2,j}-u^{2}_{1/2,j})=q^{\gamma}_{j},$$

where $q^{\gamma}_{j}=\frac{1}{|E^{\gamma}_{j}|}\int_{E^{\gamma}_{j}}q_{\gamma}(s)\,ds$.

Considering homogeneous Dirichlet boundary conditions, the equations for the normal fluxes at the horizontal boundaries are given by

$$v^{k}_{i,1/2}+2\,\frac{(K^{k}_{yy})_{i,1}}{\Delta y_1}\,p^{k}_{i,1}=0,$$

$$v^{k}_{i,N+3/2}-2\,\frac{(K^{k}_{yy})_{i,N+1}}{\Delta y_{N+1}}\,p^{k}_{i,N+1}=0,$$

$$\left(1+\frac{\beta}{d}|u^{\gamma}_{1/2}|\right)u^{\gamma}_{1/2}+2\,d\,\frac{(K^{\tau}_{f})_{1}}{\Delta y_1}\,p^{\gamma}_{1}=0,$$

$$\left(1+\frac{\beta}{d}|u^{\gamma}_{N+3/2}|\right)u^{\gamma}_{N+3/2}-2\,d\,\frac{(K^{\tau}_{f})_{N+1}}{\Delta y_{N+1}}\,p^{\gamma}_{N+1}=0.$$

In turn, the equations for the normal fluxes at the vertical boundaries take the form

$$u^{1}_{1/2,j}+2\,\frac{(K^{1}_{xx})_{1,j}}{\Delta x^{1}_{1}}\,p^{1}_{1,j}=0,$$

$$u^{2}_{N+3/2,j}-2\,\frac{(K^{2}_{xx})_{N+1,j}}{\Delta x^{2}_{N+1}}\,p^{2}_{N+1,j}=0.$$

Finally, considering the coupling condition (5e), the equations for the normal fluxes of the porous matrix at the interface γ are

$$\left(1+\frac{\xi\,a^{1}_{j}}{\alpha_{\gamma}}\right)u^{1}_{N+3/2,j}+a^{1}_{j}\,(p^{\gamma}_{j}-p^{1}_{N+1,j})+\frac{(1-\xi)\,a^{1}_{j}}{\alpha_{\gamma}}\,u^{2}_{1/2,j}=0,$$

$$\left(1+\frac{\xi\,a^{2}_{j}}{\alpha_{\gamma}}\right)u^{2}_{1/2,j}+a^{2}_{j}\,(p^{2}_{1,j}-p^{\gamma}_{j})+\frac{(1-\xi)\,a^{2}_{j}}{\alpha_{\gamma}}\,u^{1}_{N+3/2,j}=0,$$

for $j=1,\ldots,N+1$, where $a^{1}_{j}=2(K^{1}_{xx})_{N+1,j}/\Delta x^{1}_{N+1}$ and $a^{2}_{j}=2(K^{2}_{xx})_{1,j}/\Delta x^{2}_{1}$.

Suitable scaling of the previous equations results in a nonlinear saddle point problem of the form

$$\begin{pmatrix} A_1 & C^T & 0 & B_1^T & 0 & F_1^T \\ C & A_2 & 0 & 0 & B_2^T & F_2^T \\ 0 & 0 & A_\gamma(U_\gamma) & 0 & 0 & B_\gamma^T \\ B_1 & 0 & 0 & 0 & 0 & 0 \\ 0 & B_2 & 0 & 0 & 0 & 0 \\ F_1 & F_2 & B_\gamma & 0 & 0 & 0 \end{pmatrix} \begin{pmatrix} U_1 \\ U_2 \\ U_\gamma \\ P_1 \\ P_2 \\ P_\gamma \end{pmatrix} = \begin{pmatrix} 0 \\ 0 \\ 0 \\ Q_1 \\ Q_2 \\ Q_\gamma \end{pmatrix},$$

where U^1, U^2 and U^γ comprise the velocity unknowns on Ω_1, Ω_2 and γ, respectively. Similarly, P^1, P^2 and P^γ contain the pressure unknowns on Ω_1, Ω_2 and γ, respectively. The matrices A_1, A_2 and $A_\gamma(U_\gamma)$ are diagonal. It is important to notice that the nonlinearity of the problem is associated only with the one-dimensional Forchheimer equation posed on the fracture.

Remark 1. If we consider a fracture network with several intersecting fractures, we shall impose mass conservation and pressure continuity at the intersection points. In this case, the preceding system should be appropriately modified, yet preserving a nonlinear saddle point structure.

4. The monolithic multigrid method

Typically, there are two approaches for solving nonlinear problems by using multigrid techniques. One is to apply some linearization method, such as Newton's iteration or Picard method, and then to use multigrid for solving the linear problem corresponding to each iteration step. The second approach, known as full approximation scheme (FAS) [39], consists of applying multigrid directly to the nonlinear problem. This is the approach followed in this work, that is briefly described in the sequel. Remarkably, we only need to consider the two-level variant since, as for the linear case, the nonlinear FAS multigrid method can be defined recursively on the basis of this variant. In this way, if $A_h(u_h) = f_h$ denotes a nonlinear system of equations, a two-level FAS scheme reads as follows:

Full Approximation Scheme (FAS):

- Pre-smoothing: compute $\bar{u}_h^m$ by applying ν_1 smoothing steps: $\bar{u}_h^m = S_h^{\nu_1} u_h^m$.
- Restrict the residual and the current approximation to the coarse grid: $r_H = I_{h,H}(f_h - A_h(\bar{u}_h^m))$ and $u_H^m = \widetilde{I}_{h,H}\bar{u}_h^m$.
- Solve the coarse-grid problem: $A_H(v_H^m) = A_H(u_H^m) + r_H$.
- Interpolate the error approximation to the fine grid and correct the current fine grid approximation: $\hat{u}_h^m = \bar{u}_h^m + I_{H,h}(v_H^m - u_H^m)$.

- Post-smoothing: compute u_h^{m+1} by applying ν_2 smoothing steps : $u_h^{m+1} = S_h^{\nu_2}\hat{u}_h^m$.

Here, S_h denotes a nonlinear relaxation procedure, $I_{h,H}$ and $\widetilde{I}_{h,H}$ are possibly different transfer operators from the fine to the coarse grid, and $I_{H,h}$ is a transfer operator from the coarse to the fine grid. Note that, if A_h is a linear operator, then the FAS scheme is identical to the standard linear multigrid method.

In this work, we propose a monolithic multigrid method for solving the Darcy–Forchheimer flow in a fractured porous media. This means that we do not iterate between the subproblems in the matrix and within the fracture network, and we treat the whole problem at once. It is well known that the performance of a multigrid method strongly depends on its components. Notice that we are considering a nonlinear saddle point problem with a mixed-dimensional character, and this will have a great influence on the choice of the multigrid elements. Next, we describe the components used to define the nonlinear multigrid scheme.

4.1. Inter-grid transfer operators

In this section, we introduce the restriction and interpolation operators involved in the multigrid method for solving the mixed-dimensional problem. We consider different transfer operators for the unknowns belonging to the matrix and for those located at the fractures. Specifically, we choose two-dimensional and one-dimensional transfer operators, respectively. This means that we implement mixed-dimensional transfer operators in our multigrid algorithm in order to handle the problem at once.

Regarding the unknowns of the porous matrix, we take into account the staggered arrangement of their location. Therefore, the inter-grid transfer operators acting on the porous matrix unknowns are defined as follows: a six-point restriction is considered at the velocity grid points, while a four-point restriction is applied at the pressure grid points. In stencil notation, these restriction operators are given by

$$I_{h,H}^u = \frac{1}{8}\begin{pmatrix} 1 & 2 & 1 \\ & * & \\ 1 & 2 & 1 \end{pmatrix}_h, \quad I_{h,H}^v = \frac{1}{8}\begin{pmatrix} 1 & & 1 \\ 2 & * & 2 \\ 1 & & 1 \end{pmatrix}_h, \quad I_{h,H}^p = \frac{1}{4}\begin{pmatrix} 1 & & 1 \\ & * & \\ 1 & & 1 \end{pmatrix}_h,$$

respectively. We have used the same restriction operators for the current approximations, that is, $\widetilde{I}_{h,H}^u = I_{h,H}^u$, $\widetilde{I}_{h,H}^v = I_{h,H}^v$ and $\widetilde{I}_{h,H}^p = I_{h,H}^p$. Note that we choose the adjoints of the restrictions as the prolongation operators $I_{H,h}^{u/v/p}$.

Regarding the inter-grid transfer operators for the unknowns at the fractures, we again take into account their one-dimensional staggered arrangement, yielding the following restriction transfer operators

$$\widetilde{I}_{h,H}^{u^\gamma} = I_{h,H}^{u^\gamma} = \frac{1}{4}\begin{pmatrix} 1 & 2 & 1 \end{pmatrix}_h, \qquad \widetilde{I}_{h,H}^{p^\gamma} = I_{h,H}^{p^\gamma} = \frac{1}{2}\begin{pmatrix} 1 & * & 1 \end{pmatrix}_h.$$

In turn, their adjoints are considered to be the prolongation operators.

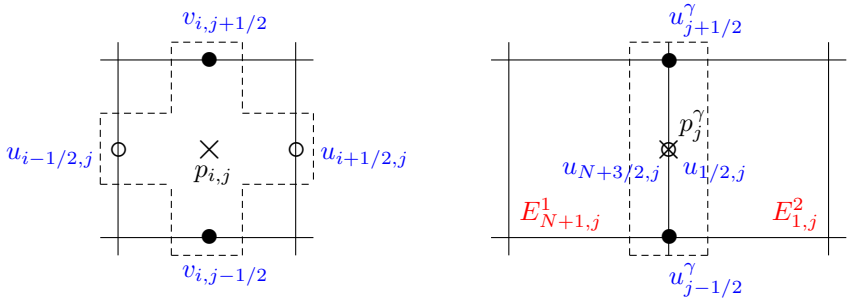

Figure 3: Unknowns updated together by the (left) two-dimensional and (right) one-dimensional Vanka-type smoothers, applied in the porous matrix and within the fractures, respectively.

4.2. Smoother

The proposed smoother is based on the well-known Vanka relaxation procedure, which was proposed by Vanka in [41] for solving the staggered finite difference discretization of the Navier–Stokes equations. This smoother was based on simultaneously updating all unknowns appearing in the discrete divergence operator in the pressure equation. Thus, the relaxation designed here for the proposed coupled problem lies in combining two- and one-dimensional Vanka-type smoothers for the unknowns in the matrix and within the fractures, respectively. Moreover, at each smoothing step, two relaxations of the one-dimensional Vanka smoother, with a relaxation parameter $w = 0.7$, are performed within the fractures, whereas only one smoothing iteration of the two-dimensional Vanka relaxation is carried out in the matrix. Notice that the computational cost of the smoothing step in the fracture is negligible in comparison with that of the porous matrix, since it is a one-dimensional calculation.

More concretely, in the case of the porous matrix, the Vanka smoothing approach implies that four velocity unknowns and one pressure unknown are simultaneously updated (see Figure 3, left). This means that we iterate over all cells at each two-dimensional smoothing step, and a 5×5 system is solved on each cell. In terms of increments, such a system is written as

$$\begin{pmatrix} 1 & 0 & 0 & 0 & -\frac{K_{xx}}{h} \\ 0 & 1 & 0 & 0 & \frac{K_{xx}}{h} \\ 0 & 0 & 1 & 0 & -\frac{K_{yy}}{h} \\ 0 & 0 & 0 & 1 & \frac{K_{yy}}{h} \\ \frac{1}{h} & -\frac{1}{h} & \frac{1}{h} & -\frac{1}{h} & 0 \end{pmatrix} \begin{pmatrix} \delta u_{i+1/2,j} \\ \delta u_{i-1/2,j} \\ \delta v_{i,j+1/2} \\ \delta v_{i,j-1/2} \\ \delta p_{i,j} \end{pmatrix} = \begin{pmatrix} r^{u}_{i+1/2,j} \\ r^{u}_{i-1/2,j} \\ r^{v}_{i,j+1/2} \\ r^{v}_{i,j-1/2} \\ r^{p}_{i,j} \end{pmatrix}.$$

For the sake of simplicity, in the previous system we omitted the superscript k indicating the corresponding subdomain, we considered a uniform grid in both directions, with mesh size h, and we assumed that the permeability tensors are homogeneous on the corresponding subdomain.

Regarding the one-dimensional Vanka smoother within the fractures, three fracture unknowns are simultaneously updated on each cell –those corresponding

to the pressure and the velocities associated to the cell–, together with two velocities from the porous matrix which are located at the same point as the fracture pressure (see Figure 3, right). In this way, a 5×5 system has to be solved for each pressure grid point. In particular, for the case of one vertical fracture considered in Section 3, the system to solve takes the form

$$\begin{pmatrix} 1+\frac{\beta}{d}|u^{\gamma}_{j+1/2}| & 0 & -d\frac{K^{\tau}_f}{h} & 0 & 0 \\ 0 & 1+\frac{\beta}{d}|u^{\gamma}_{j-1/2}| & d\frac{K^{\tau}_f}{h} & 0 & 0 \\ \frac{1}{h} & -\frac{1}{h} & 0 & -1 & 1 \\ 0 & 0 & a^1_j & 1+\frac{\xi a^1_j}{\alpha_\gamma} & \frac{(1-\xi)a^1_j}{\alpha_\gamma} \\ 0 & 0 & -a^2_j & \frac{(1-\xi)a^2_j}{\alpha_\gamma} & 1+\frac{\xi a^2_j}{\alpha_\gamma} \end{pmatrix} \begin{pmatrix} \delta u^{\gamma}_{j+1/2} \\ \delta u^{\gamma}_{j-1/2} \\ \delta p^{\gamma}_j \\ \delta u^1_{N+3/2,j} \\ \delta u^2_{1/2,j} \end{pmatrix} = \begin{pmatrix} \delta r^{u^\gamma}_{j+1/2} \\ \delta r^{u^\gamma}_{j-1/2} \\ \delta r^{p^\gamma}_j \\ \delta r^{u^1}_{N+3/2,j} \\ \delta r^{u^2}_{1/2,j} \end{pmatrix},$$

where h denotes the uniform mesh size, K^{τ}_f is assumed constant along the fracture, and the rest of the parameters are those defined in Section 3. Here, the nonlinearity is handled via a Picard iteration, namely: the diagonal elements of the previous matrix are computed by using the velocities at the previous smoothing step. Finally, we apply a block Gauss–Seidel smoother coupling the fracture velocity unknowns located at each intersection point between fractures, if any.

4.3. Computational cost

It is well known that, in general, the most time-consuming part of a multigrid algorithm is the smoothing procedure. In our case, this is even more noticeable due to the fact that the chosen smoother has to solve small dense systems of equations for each grid point. In particular, for the proposed mixed-dimensional multigrid method, the most demanding part in terms of CPU time is the relaxation method in the two-dimensional porous matrix. Hence, we can get an idea of the computational complexity of the method by looking at the complexity of the proposed two-dimensional Vanka smoother. In the porous matrix, this Vanka smoother requires the solution of small 5×5 dense systems for each pressure degree of freedom. The most expensive parts of this smoothing iteration are the matrix-vector multiplications required to calculate the local residual and the solution of each dense system. By using a standard approach, the cost of the computation of each local defect is $\mathcal{O}(n)$, where n is the total number of degrees of freedom. In turn, the cost of solving the system depends on the chosen method: assuming that the inverse of the system matrix is stored or the resulting L and U factors are stored in a block LU-factorization, the cost of calculating the correction is $\mathcal{O}(n)$ too. As a consequence, the global computational cost per iteration of the multiplicative Schwarz smoother is $\mathcal{O}(n)$.

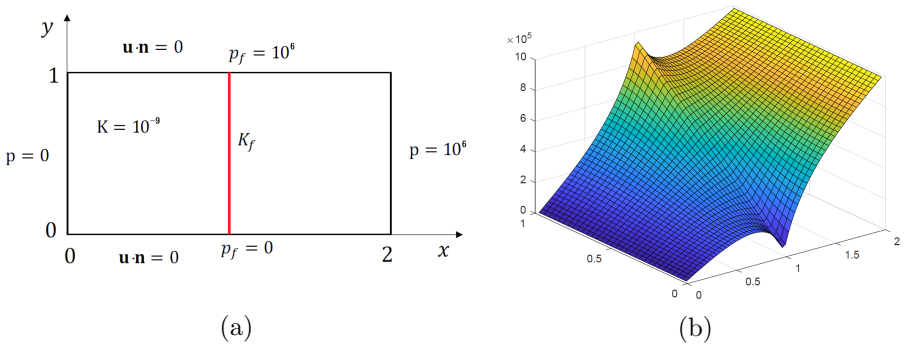

(a) (b)

Figure 4: (a) Domain and boundary conditions and (b) pressure solution for the case $K_f = 10^{-6}$ and $\beta = 10$.

Remark 2. The proposed method can be straightforwardly extended to solve three-dimensional problems with an arbitrary fracture network composed of possibly intersecting horizontal and/or vertical planar fractures. In this case, the mixed-dimensional multigrid method would combine two- and three-dimensional smoothers and inter-grid transfer operators within the fractures and the porous matrix, respectively. Moreover, we could use a one-dimensional smoother, or even a direct solver, at the intersections of fractures. We would expect very successful results as in the two-dimensional case presented here. However, the implementation of a three-dimensional model that considers intersecting fractures could easily become quite involved.

5. Numerical experiments

In this section, we present some numerical experiments to show the robustness and the efficiency of the proposed multigrid method for the interface model. In all the tests, we apply the FAS multigrid method based on the Vanka-type smoothers described in Section 4.2. At each smoothing step, we apply one iteration of the Vanka strategy in the porous medium and two iterations within the fracture, considering a damping parameter $w = 0.7$. Note that, in this model, the fracture is considered to be a one-dimensional object, so that the computational cost of calculating the fracture unknowns is negligible as compared to that of solving the problem in the porous medium. We use W-cycles with two pre- and two post-smoothing steps, since this choice was shown to provide very good results for solving complex coupled problems like the Darcy–Stokes system [45], the Biot–Stokes system [46] and the single phase Darcy–Darcy coupling between the fractures and the porous matrix [38]. All our numerical computations are carried out using MATLAB.

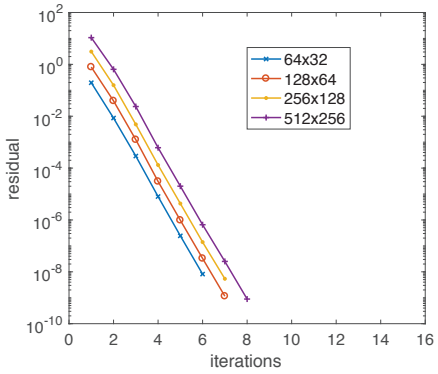

Figure 5: History of convergence for the monolithic multigrid method if $K_f = 10^{-6}$ and $\beta = 10$.

5.1. A single fracture test

First, we consider a test problem presented in [33], where the domain consists of a horizontal rectangular slice of porous medium $\Omega = (0, 2) \times (0, 1)$. Such a domain is divided into two equally-sized subdomains by a vertical fracture Ω_f of unit length and width $d = 0.01$. The permeability in the porous medium is assumed to be $\mathbf{K} = K\mathbf{I}$, where $K = 10^{-9}$ and $\mathbf{I}$ stands for the identity matrix. In turn, the permeability in the fracture is given by $\mathbf{K}_f = K_f\mathbf{I}$, where $K_f = K_f^{\boldsymbol{\tau}} = K_f^{\mathbf{n}}$ is supposed to be greater than K. We will perform several numerical tests for different values of the permeability K_f, as well as for different values of the Forchheimer coefficient β. The upper and lower boundaries of the porous medium are assumed to be impermeable. Pressure is fixed to the values $p = 0$ and $p = 10^6$ on the left and right boundaries, respectively. The boundary conditions of the fracture are of Dirichlet type. More precisely, $p_f = 10^6$ on the top extremity of the fracture and $p_f = 0$ on the bottom. All these settings are displayed on Figure 4 (a). For illustration, we show the pressure solution obtained for a fracture permeability $K_f = 10^{-6}$ and a Forchheimer coefficient $\beta = 10$ in Figure 4 (b). The problem has been discretized using the finite volume scheme described in Section 3, considering a uniform grid in both directions with mesh size h.

Throughout this subsection, we show the robustness of the monolithic mixed-dimensional multigrid method with respect to the spatial discretization parameter h, the permeability of the fracture K_f, and the Forchheimer coefficient β. Note that the problem becomes harder to solve as the permeability of the fracture K_f increases, mainly because of the bigger jump between this permeability and that of the porous matrix. In addition, the solution of the mixed-dimensional coupled problem becomes more involved as the coefficient β increases, since this coefficient enhances the nonlinearity.

We study the performance of the monolithic mixed-dimensional multigrid method by fixing the permeability of the fracture to $K_f = 10^{-6}$ and the Forch-

K_f	$h^{-1} = 32$	$h^{-1} = 64$	$h^{-1} = 128$	$h^{-1} = 256$
10^{-6}	8	8	8	9
10^{-4}	9	9	9	9
10^{-2}	9	9	9	10
1	10	10	11	11

Table 1: Number of $W(2,2)$-iterations of the FAS multigrid method required to reduce the initial residual by a factor of 10^{-10}, for different values of the permeability in the fracture K_f and for different mesh sizes. The Forchheimer coefficient is $\beta = 10$ and a single fracture is considered.

heimer coefficient to $\beta = 10$. In Figure 5, we display the history of convergence of the multigrid solver for different mesh sizes. In particular, the reduction of the residual is depicted versus the number of iterations, while the stopping criterion is set to reduce the initial residual to 10^{-8}. It can be observed that the convergence of the multigrid method is independent of the spatial discretization parameter. Moreover, it results in a very efficient solver, since only around 8 iterations are needed to solve the nonlinear mixed-dimensional coupled problem.

Next, we set the Forchheimer coefficient to be $\beta = 10$ in order to study the robustness of the multigrid solver with respect to different values of the permeability of the fracture K_f. In Table 1, we display the number of iterations needed to reduce the initial residual by a factor of 10^{-10}, for different grid sizes and permeability values. We can observe that, for all the considered values of K_f, the performance of the multigrid method is independent of the spatial discretization parameter. Further, the number of iterations needed to satisfy the stopping criterion is kept to a small quantity.

Finally, Table 2 shows the number of iterations required to reduce the initial residual by a factor of 10^{-10}, for different values of the Forchheimer coefficient β and for different grid sizes. In this case, we fix the permeability of the fracture to the value $K_f = 10^{-6}$. As mentioned above, the parameter β controls the strength of the nonlinearity, thus implying that the bigger β, the harder the problem we solve. For comparison, we have also included the case $\beta = 0$, corresponding to Darcy's law within the fracture. It is well known that the FAS scheme for linear problems is theoretically equivalent to the usual linear multigrid scheme [40]. In such a case, the resulting multigrid method is similar to that proposed in [38] for solving a single-phase Darcy–Darcy coupling in a fractured porous medium. The numerical results indicate that the performance of the solver is very similar for all the cases under consideration, i.e., the multigrid method is also robust with respect to the Forchheimer coefficient β.

5.2. Two intersecting fractures

The aim of this numerical test is to discuss the performance of the proposed multigrid method when several fractures are considered. In particular, the fracture network in this example consists of two crossing fractures, and the results

β	$h^{-1} = 32$	$h^{-1} = 64$	$h^{-1} = 128$	$h^{-1} = 256$
0	8	8	8	9
10	8	8	8	9
50	8	9	9	10
100	9	9	10	10
200	10	10	10	10

Table 2: Number of $W(2,2)$-iterations of the FAS multigrid method required to reduce the initial residual by a factor of 10^{-10}, for different values of the Forchheimer coefficient β and for different mesh sizes. The permeability in the fracture is $K_f = 10^{-6}$ and a single fracture is considered.

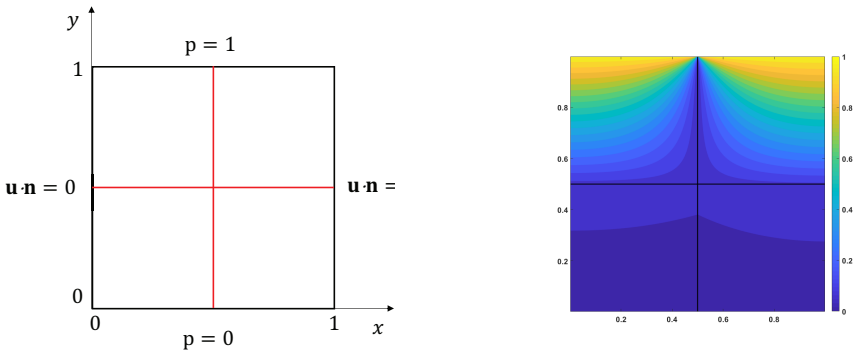

(a) (b)

Figure 6: (a) Fracture network and settings, and (b) pressure solution for the case $K_f = 10^{-3}$ and $\beta = 100$.

shown below indicate that the treatment of the intersection points between fractures provides a robust solver. The computational domain in this example is the unit square, with impermeable lateral walls and a given pressure on the top ($p = 1$) and bottom ($p = 0$) boundaries. As shown in Figure 6 (a), this flow domain is divided into four equally-sized squares by two crossing fractures. The permeabilities in the porous matrix and the fractures are considered to be diagonal tensors, given by $\mathbf{K} = 10^{-6}(1 + xy)\,\mathbf{I}$ and $\mathbf{K}_f = K_f\,\mathbf{I}$, respectively. Unlike the previous experiment, this example considers heterogeneous permeability tensors in the porous matrix. In Figure 6 (b), we show the pressure solution for $K_f = 10^{-3}$.

First, we illustrate the robustness of the proposed algorithm with respect to the value of the permeability in the fracture. In Table 3, the number of FAS iterations required to reduce the initial residual by a factor of 10^{-10} are shown, for different values of K_f. Furthermore, we can also see that the convergence of the proposed multigrid method is independent of the discretization parameter, since the number of iterations remains constant for different mesh sizes. In this

K_f	$h^{-1}=32$	$h^{-1}=64$	$h^{-1}=128$	$h^{-1}=256$
10^{-6}	9	9	9	9
10^{-4}	9	9	9	9
10^{-2}	9	9	9	9
1	9	9	9	9

Table 3: Number of $W(2,2)$-iterations of the FAS multigrid method required to reduce the initial residual by a factor of 10^{-10}, for different values of the permeability in the fractures K_f and for different mesh sizes. The Forchheimer coefficient is $\beta = 100$ and two intersecting fractures are considered.

β	$h^{-1}=32$	$h^{-1}=64$	$h^{-1}=128$	$h^{-1}=256$
0	9	9	9	9
10	9	9	9	9
50	9	9	9	9
100	9	9	9	9
200	9	9	9	9

Table 4: Number of $W(2,2)$-iterations of the FAS multigrid method required to reduce the initial residual by a factor of 10^{-10}, for different values of the Forchheimer coefficient β and for different mesh sizes. The permeability in the fractures is $K_f = 10^{-3}$ and two intersecting fractures are considered.

example, the Forchheimer coefficient is fixed to $\beta = 100$.

Next, as in the case of a single fracture, we test the performance of our solver for different values of the Forchheimer parameter. For this purpose, we set the permeability in the fracture to a value $K_f = 10^{-3}$. In Table 4, the number of FAS iterations required to reduce the initial residual by a factor of 10^{-10} are shown, for different values of β and for several mesh sizes. It is clear from the results that the proposed nonlinear multigrid method is robust with respect to such parameters. Remarkably, the stopping criterion is achieved after a small number of iterations, even when the Forchheimer parameter is large (that is, when the problem is strongly nonlinear).

Finally, we study the effect of an increasing in the injection rate for one of the fractures. In particular, we consider the same configuration as that shown in Figure 6 (a), but now assuming a non-homogeneous Dirichlet boundary condition p_f for the vertical fracture at the North boundary. Table 5 shows the number of iterations required by the FAS algorithm to reduce the initial residual by a factor of 10^{-10}, for different values of p_f and for several mesh sizes. In this case, we observe that the performance of the multigrid method is not affected by the Dirichlet boundary data imposed on the fracture.

p_f	$h^{-1}=32$	$h^{-1}=64$	$h^{-1}=128$	$h^{-1}=256$
10^1	8	9	9	9
10^2	8	9	9	9
10^3	9	9	10	11

Table 5: Number of $W(2,2)$-iterations of the FAS multigrid method required to reduce the initial residual by a factor of 10^{-10}, for different values of the Dirichlet boundary data p_f and for different mesh sizes. The permeability in the fracture is $K_f = 10^{-4}$, the Forchheimer coefficient is $\beta = 100$ and two intersecting fractures are considered.

Acknowledgements

Francisco J. Gaspar has received funding from the European Union's Horizon 2020 research and innovation programme under the Marie Skłodowska-Curie grant agreement No. 705402, POROSOS. The work of Carmen Rodrigo is supported in part by the FEDER/MINECO project MTM2016-75139-R. The work of Andrés Arrarás and Laura Portero is supported in part by the FEDER/MINECO projects MTM2014-52859-P and MTM2016-75139-R.

References

[1] G. I. Barenblatt, I. P. Zheltov, I. N. Kochina, Basic concepts in the theory of seepage of homogeneous liquids in fissured rocks [strata], Prikl. Mat. Mekh. 24 (1960) 852–864 (in Russian), English transl. J. Appl. Math. Mech. 24 (1960) 1286–1303.

[2] T. Arbogast, J. Douglas, Jr., U. Hornung, Derivation of the double porosity model of single phase flow via homogenization theory, SIAM J. Math. Anal. 21 (1990) 823–836.

[3] L. Formaggia, A. Fumagalli, A. Scotti, P. Ruffo, A reduced model for Darcy's problem in networks of fractures, ESAIM Math. Model. Numer. Anal. 48 (2014) 1089–1116.

[4] G. Pichot, J. Erhel, J.-R. de Dreuzy, A generalized mixed hybrid mortar method for solving flow in stochastic discrete fracture networks, SIAM J. Sci. Comput. 34 (2012) B86–B105.

[5] M. F. Benedetto, S. Berrone, S. Pieraccini, S. Scialò, The virtual element method for discrete fracture network simulations, Comput. Methods Appl. Mech. Engrg. 280 (2014) 135–156.

[6] E. Keilegavlen, A. Fumagalli, R. Berge, I. Stefansson, Implementation of mixed-dimensional models for flow in fractured porous media, arXiv:1712.07392 [cs.CE], 2017.

[7] V. Martin, J. Jaffré, J. E. Roberts, Modeling fractures and barriers as interfaces for flow in porous media, SIAM J. Sci. Comp. 26 (2005) 1667–1691.

[8] B. Flemisch, A. Fumagalli, A. Scotti, A review of the XFEM-based approximation of flow in fractured porous media, in: Advances in Discretization Methods, Vol. 12 of SEMA SIMAI Springer Ser., Springer, Cham, 2016, pp. 47–76.

[9] M. Del Pra, A. Fumagalli, A. Scotti, Well posedness of fully coupled fracture/bulk Darcy flow with XFEM, SIAM J. Numer. Anal. 55 (2017) 785–811.

[10] N. Frih, V. Martin, J. E. Roberts, A. Saâda, Modeling fractures as interfaces with nonmatching grids, Comput. Geosci. 16 (2012) 1043–1060.

[11] M. Balhoff, A. Mikelić, M. F. Wheeler, Polynomial filtration laws for low Reynolds number flows through porous media, Transp. Porous Media 81 (2010) 35–60.

[12] J. Geertsma, Estimating the coefficient of inertial resistance in fluid flow through porous media, SPE J. 14 (1974) 445–450.

[13] C. C. Mei, J.-L. Auriault, The effect of weak inertia on flow through a porous medium, J. Fluid Mech. 222 (1991) 647–663.

[14] M. Panfilov, M. Fourar, Physical splitting of nonlinear effects in high-velocity stable flow through porous media, Adv. Water Resour. 29 (2006) 30–41.

[15] H. Huang, J. A. Ayoub, Applicability of the Forchheimer equation for non-Darcy flow in porous media, SPE J. 13 (2008) 112–122.

[16] R. D. Barree, M. W. Conway, Beyond beta factors: a complete model for Darcy, Forchheimer, and Trans-Forchheimer flow in porous media, in: SPE Annual Technical Conference and Exhibition, SPE 89325, Houston, 2004, pp. 1–8.

[17] Z. Chen, S. L. Lyons, G. Qin, Derivation of the Forchheimer law via homogenization, Transp. Porous Media 44 (2001) 325–335.

[18] T. Giorgi, Derivation of the Forchheimer law via matched asymptotic expansions, Transp. Porous Media 29 (1997) 191–206.

[19] D. Ruth, H. Ma, On the derivation of the Forchheimer equation by means of the averaging theorem, Transp. Porous Media 7 (1992) 255–264.

[20] S. Whitaker, The Forchheimer equation: a theoretical development, Transp. Porous Media 25 (1996) 27–61.

[21] S. M. Hassanizadeh, W. G. Gray, High velocity flow in porous media, Transp. Porous Media 2 (1987) 521–531.

[22] Y. Amirat, Écoulements en milieu poreux n'obéissant pas à la loi de Darcy, RAIRO Modél. Math. Anal. Numér. 25 (1991) 273–306.

[23] P. Fabrie, Regularity of the solution of Darcy–Forchheimer's equation, Nonlinear Anal. 13 (1989) 1025–1049.

[24] P. Knabner, G. Summ, Solvability of the mixed formulation for Darcy–Forchheimer flow in porous media, arXiv:1608.08829 [math.NA], 2016.

[25] J. Douglas, Jr., P. J. Paes-Leme, T. Giorgi, Generalized Forchheimer flow in porous media, in: J.-L. Lions, C. Baiocchi (Eds.), Boundary value problems for partial differential equations and applications, Vol. 29 of RMA Res. Notes Appl. Math., Masson, Paris, 1993, pp. 99–111.

[26] T. T. Kieu, Analysis of expanded mixed finite element methods for the generalized Forchheimer flows of slightly compressible fluids, Numer. Methods Partial Differential Equations 32 (2016) 60–85.

[27] E.-J. Park, Mixed finite element methods for generalized Forchheimer flow in porous media, Numer. Methods Partial Differential Equations 21 (2005) 213–228.

[28] H. Rui, H. Pan, A block-centered finite difference method for the Darcy-Forchheimer model, SIAM J. Numer. Anal. 50 (2012) 2612–2631.

[29] H. Rui, H. Pan, A block-centered finite difference method for slightly compressible Darcy–Forchheimer flow in porous media, J. Sci. Comput. 73 (2017) 70–92.

[30] W. Xu, D. Liang, H. Rui, A multipoint flux mixed finite element method for the compressible Darcy–Forchheimer models, Appl. Math. Comput. 315 (2017) 259–277.

[31] P. Knabner, J. E. Roberts, Mathematical analysis of a discrete fracture model coupling Darcy flow in the matrix with Darcy–Forchheimer flow in the fracture, ESAIM Math. Model. Numer. Anal. 48 (2014) 1451–1472.

[32] N. Frih, J. E. Roberts, A. Saada, Un modèle Darcy–Forchheimer pour un écoulement dans un milieu poreux fracturé, ARIMA 5 (2006) 129–143.

[33] N. Frih, J. E. Roberts, A. Saada, Modeling fractures as interfaces: a model for Forchheimer fractures, Comput. Geosci. 12 (2008) 91–104.

[34] V. Girault, M. F. Wheeler, Numerical discretization of a Darcy–Forchheimer model, Numer. Math. 110 (2008) 161–198.

[35] H. Rui, W. Liu, A two-grid block-centered finite difference method for Darcy–Forchheimer flow in porous media, SIAM J. Numer. Anal. 53 (2015) 1941–1962.

[36] M. Sun, H. Rui, A two-grid stabilized mixed finite element method for Darcy-Forchheimer model, Numer. Methods Partial Differential Equations 34 (2018) 686–704.

[37] J. Huang, L. Chen, H. Rui, Multigrid methods for a mixed finite element method of the Darcy–Forchheimer model, J. Sci. Comput. 74 (2018) 396–411.

[38] A. Arrarás, F. J. Gaspar, L. Portero, C. Rodrigo, Mixed-dimensional multigrid methods for fractured porous media, Submitted.

[39] A. Brandt, Multi-level adaptive solutions to boundary-value problems, Math. Comp. 31 (1977) 333–390.

[40] U. Trottenberg, C. W. Oosterlee, A. Schüller, Multigrid, Academic Press, New York, 2001.

[41] S. P. Vanka, Block-implicit multigrid solution of Navier-Stokes equations in primitive variables, J. Comput. Phys. 65 (1986) 138–158.

[42] P. Angot, F. Boyer, F. Hubert, Asymptotic and numerical modelling of flows in fractured porous media, M2AN Math. Model. Numer. Anal. 43 (2009) 239–275.

[43] C. D'Angelo, A. Scotti, A mixed finite element method for Darcy flow in fractured porous media with non-matching grids, ESAIM Math. Model. Numer. Anal. 46 (2012) 465–489.

[44] R. Eymard, T. Gallouët, C. Guichard, R. Herbin, R. Masson, TP or not TP, that is the question, Comput. Geosci. 18 (2014) 285–296.

[45] P. Luo, C. Rodrigo, F. J. Gaspar, C. W. Oosterlee, Uzawa smoother in multigrid for the coupled porous medium and Stokes flow system, SIAM J. Sci. Comp. 39 (2017) S633–S661.

[46] P. Luo, C. Rodrigo, F. J. Gaspar, C. W. Oosterlee, Monolithic multigrid method for the coupled Stokes flow and deformable porous medium system, J. Comput. Phys. 353 (2018) 148–168.